

1 **Impact of vehicular emissions on the formation of fine particles in the Sao Paulo**
2 **Metropolitan Area: A numerical study with the WRF-Chem model**

3

4 **Angel Vara-Vela¹, M. F. Andrade¹, Prashant Kumar^{2,3}, R. Y. Ynoue¹, and A. G.**
5 **Muñoz^{4,5}**

6

7 ¹Department of Atmospheric Sciences, Institute of Astronomy, Geophysics and
8 Atmospheric Sciences, University of Sao Paulo, Sao Paulo, Brazil

9 ²Department of Civil and Environmental Engineering, Faculty of Engineering and
10 Physical Sciences (FEPS), University of Surrey, Guilford GU2 7XH, United Kingdom

11 ³Environmental Flow (EnFlo) Research Centre, Faculty of Engineering and Physical
12 Sciences, University of Surrey, Guildford GU2 7XH, United Kingdom

13 ⁴International Research Institute for Climate and Society (IRI), The Earth Institute,
14 Columbia University, NY, USA

15 ⁵Centro de Modelado Científico (CMC), Universidad del Zulia, Maracaibo, Venezuela
16

17 Corresponding author: A. V. Vela (angel.vela@iag.usp.br)

18

19 **Abstract**

20 The objective of this work is to evaluate the impact of vehicular emissions on the
21 formation of fine particles (PM_{2.5}; ≤2.5 μm in diameter) in the Sao Paulo Metropolitan
22 Area (SPMA) in Brazil, where ethanol is used intensively as a fuel in road vehicles. The
23 Weather Research and Forecasting with Chemistry (WRF-Chem) model, which
24 simulates feedbacks between meteorological variables and chemical species, is used as
25 photochemical modelling tool to describe the physico-chemical processes leading to

1

26 evolution of number and mass size distribution of particles through gas-to-particle
27 conversion. A vehicular emission model based on statistical information of vehicular
28 activity is applied to simulate vehicular emissions over the studied area. The simulation
29 has been performed for a one month period (7 August - 6 September 2012) to cover the
30 availability of experimental data from the NUANCE-SPS (Narrowing the Uncertainties
31 on Aerosol and Climate Changes in Sao Paulo State) project that aims to characterize
32 emissions of atmospheric aerosols in the SPMA. The availability of experimental
33 measurements of atmospheric aerosols and the application of the WRF-Chem model
34 made it possible to represent some of the most important properties of fine particles in
35 the SPMA such as the mass size distribution and chemical composition, besides
36 allowing us to evaluate its formation potential through the gas-to-particle conversion
37 processes. Results show that the emission of primary gases, mostly from vehicles, led to
38 a production of secondary particles between 20 and 30 % in relation to the total mass
39 concentration of $PM_{2.5}$ in the downtown SPMA. Each of $PM_{2.5}$ and primary natural
40 aerosol (dust and sea salt) contributed with 40-50% of the total PM_{10} (i.e. those $\leq 10 \mu m$
41 in diameter) concentration. Over 40% of the formation of fine particles, by mass, was
42 due to the emission of hydrocarbons, mainly aromatics. Furthermore, an increase in the
43 number of small particles impaired the ultraviolet radiation and induced a decrease in
44 ozone formation. The ground level O_3 concentration decreased by about 2% when the
45 aerosol-radiation feedback is taken into account.

46

47 **1. Introduction**

48 The Sao Paulo Metropolitan Area (SPMA), in the southeast region of Brazil, is
49 considered a megalopolis comprised of Sao Paulo city and more 38 municipalities. One
50 of the main concern in the SPMA is the occurrence of violations of air quality standards

51 for ozone and fine particles at different air quality stations from the Sao Paulo
52 Environmental Agency (CETESB). The air pollutant emissions in the SPMA are related
53 to the burning of the fuels: ethanol, gasohol (gasoline with 25% ethanol) and diesel.
54 Recent work of Carvalho et al. (2014) reported a substantial increase in number of road
55 vehicles from 1 million in 2000 to almost 7 million in 2014, together with an overview
56 of the pollutants concentration, fuel use in the SPMA and the relationship between the
57 emissions and the improvement in the air quality in past years.

58 They constitute the main cause of impairment to air quality in the SPMA, but
59 the number of air quality standard violations has decreased for almost all pollutants with
60 the exception of $PM_{2.5}$ and O_3 . Both these pollutants are impacted by the vehicular
61 emissions and have experienced an increase in the number of violations of local air
62 quality standards as discussed in detail by Carvalho et al. (2014). Pérez-Martínez et al.
63 (2015) have analyzed the monthly mean values for the regulated pollutants from 2000 to
64 2013 for the air quality stations in the SPMA. They found a decrease in the average
65 concentration of NO_x , CO and PM_{10} by 0.65, 0.37 and 0.71 % month⁻¹, respectively,
66 although the sales of the fuels (gasoline, ethanol, and diesel) had increased by 0.26, 1.96
67 and 0.38 % month⁻¹, respectively.

68 A recent report from CETESB (CETESB, 2013) highlighted that, in 2012, the
69 vehicles contributed with about 40% of the total PM_{10} mass concentrations through
70 direct emissions. If we consider the secondary aerosols, which were about 25% of PM_{10}
71 as estimated by CETESB (2013), these were mainly found to be formed by chemical
72 reactions between gases released from exhaust of vehicles.

73 The implementation of the Program for the Control of Vehicular Emission
74 (PROCONVE) established by the Brazilian Government in the 80's, enforcing measures
75 such as use of catalytic converters and ethanol as additive to gasoline in substitution of

76 tetraethyllead, led to decrease in emissions of CO and VOCs and hence their ambient
77 concentration. Although the emissions have been controlled by regulations, the number
78 of vehicles has increased substantially and faster than the replacement of the old
79 vehicles by the new ones (Pérez-Martínez et al., 2014). According to CETESB (2013),
80 the road vehicles contributed up to about 97, 87 and 80% of CO, VOCs and NO_x
81 emissions in 2012, respectively, being most of NO_x associated to diesel combustion and
82 most of CO and VOCs from gasohol and ethanol combustion. Receptor modelling
83 studies applied to six capital cities in Brazil (Andrade et al., 2012) showed that only
84 13% of PM_{2.5} in the SPMA is associated to the emission by the industrial processes (oil
85 burning and secondary aerosols).

86 To date, many studies assessing the impact of biofuels on the air quality have
87 been performed in Brazil. For example, Anderson (2009) conducted a review
88 concerning the use of ethanol fuel in Brazil. His work highlighted that the atmospheric
89 concentrations of acetaldehyde and ethanol are much higher in Brazil in comparison
90 with the other areas of the world. Costa and Sodré (2010) showed that exhaust
91 emissions of hydrous ethanol reduced CO and Hydrocarbons (HC), but increased CO₂
92 and NO_x levels.

93 A number of past studies has shown the significant participation of the
94 carbonaceous compounds in the concentration of fine particles in the SPMA
95 (Albuquerque et al., 2011; Miranda and Andrade, 2005; Ynoue and Andrade, 2004;
96 Castanho and Artaxo, 2001). Studies conducted on ambient air pollution in the SPMA
97 have also shown that BC explains 21% of mass concentrations of fine particles (PM_{2.5};
98 ≤2.5 μm in diameter) compared with 40% of organic carbon (OC), 20% of sulfates, and
99 12% of soil dust (Andrade et al., 2012). Most of the observed ambient PM_{2.5} mass
100 concentration usually originates from precursors gases such as sulphur dioxide (SO₂),

101 ammonia (NH₃), nitrogen oxides (NO_x) and volatile organic compounds (VOCs) as well
102 as through the physico-chemical processes such as the oxidation of low volatile
103 hydrocarbons noted above transferring to the condensed phase (McMurry et al., 2004;
104 Heal et al., 2012). Since these processes are often photo-chemically driven, the resultant
105 aerosol usually falls into the category of secondary photochemical pollutant (Jenkin and
106 Clemitshaw, 2000). Oxidation of VOCs can produce species of sufficiently low vapor
107 pressure to be condensable, leading to the formation of secondary organic aerosol
108 (SOA) (Kroll and Seinfeld, 2008). Fine particles in SPMA have a great participation on
109 its composition of SOA, formed from the emissions of VOCs, which have the same
110 origin of the primary compounds involved in the formation of ozone, from the burning
111 of fuels. The participation of the biogenic emission is considered to be small in the
112 formation of particles in the metropolitan area of the city according to previous studies
113 of Martins et al. (2006).

114 The impact of the fine particles has been discussed in previous works, with
115 evaluation of the scattering and absorbing effects of the aerosol (e.g. Li et al., 2005;
116 Real et al., 2011). Vehicular emissions of particulate matter (PM) in the SPMA have a
117 high percentage of BC (Brito et al., 2013), which after emitted to the atmosphere can
118 enhance the absorption coefficient and thus the attenuation rates.

119 One of the most important aspects of this work is the quantitative analysis of the
120 formation of PM_{2.5} and ozone (O₃) in the SPMA. Photolysis of O₃ by ultraviolet light in
121 the presence of water vapor is the main source of hydroxyl radical (OH), the most
122 important radical in the atmosphere in terms of reactivity (Monks, 2004). At the same
123 time, OH levels in the atmosphere directly determine the oxidation rate of the precursors
124 of secondary aerosols. Oxidation products of VOCs and semi-VOCs by OH are the most
125 important precursors of SOA (Li et al., 2011a). Although VOCs and NO_x are precursors

126 of both O₃ and a fraction of atmospheric PM (NO₃⁻ and secondary organics) while they
127 influence indirectly the formation of the rest of the secondary PM components like
128 SO₄⁼, their control strategies that are optimal for O₃ controls may even increase PM_{2.5}
129 concentrations (McMurry et al., 2004). Such an analysis is important to evaluate the
130 contribution of the vehicular fleet using different kind of fuels to the concentration of
131 fine particles. In this sense, a numerical study with an adequate physical approach,
132 representing particles in the modelling system, is important to understand the formation
133 of secondary aerosols from primary emission of gases in a metropolitan area where the
134 composition of fuel in vehicular fleet has changed significantly over the past years.
135 Therefore, the goal of the present study is to evaluate the impact of vehicular emissions
136 on the formation of fine particles in the SPMA, focusing especially on the potential
137 formation of secondary particles from the primary emission of gases coming from
138 on-road vehicles. The impact of aerosol particles on the ozone photochemistry is also
139 examined by means of numerical simulations. Measurements were performed to provide
140 input data to evaluate the modelling performance and estimate the vehicular emission
141 factors. Aerosol measurements were taken from field campaigns that were carried out as
142 part of the Narrowing the Uncertainties on Aerosol and Climate Changes in Sao Paulo
143 State (NUANCE-SPS) project (<http://nuance-lapat.iag.usp.br/>). These campaigns took
144 place between July and September 2012. An online-coupled meteorology and chemistry
145 model, i.e., the Weather Research and Forecasting with Chemistry (WRF-Chem) model,
146 has been used to characterize and describe the physico-chemical processes involved in
147 both the formation and growth of new particles over the SPMA in southern Brazil. The
148 details of the experimental campaigns, WRF-Chem model and emissions are described
149 in Section 2. Results from modelling experiments and comparison with measurements
150 are presented in Section 3. Finally, the summary and conclusions are given in Section 4.

151

152 **2. Methodology**

153 **2.1. Observational datasets**

154 The study period starting from 7 August until 6 September 2012 was selected for
155 comparison with the modelled results (Section 2.2) due to the availability of
156 experimental data from the NUANCE-SPS project. The aim of NUANCE-SPS was to
157 evaluate the impact of emissions in the SPMA on the air quality and changing climatic
158 conditions, and feedback mechanisms between climatic perturbations produced by both
159 primary and secondary emissions and urban atmospheric processes. Aerosol observation
160 datasets used in this work were collected using a Dichotomous sampler (Wedding et al.,
161 1980) and a Micro-Orifice Uniform Deposit Impactor (MOUDI, model 100; MSP
162 Corporation - Marple et al., 1986). The MOUDI impactor collected particles in 10 size
163 classes with nominal 50% cut-off diameters: 10, 5.6, 3.2, 1.8, 1.0, 0.56, 0.32, 0.18, 0.1
164 and 0.06 μm . Particles smaller than 0.06 μm were collected in a subsequent stage or
165 after-filter. The samples collected with the MOUDI impactor were deposited on a
166 polycarbonate membrane filter with 0.4 μm porous and for the Dichotomous sampler
167 the substrate was a teflon membrane filter with 2 μm porous. The after-filter in the
168 MOUDI impactor is a 33 mm teflon membrane filter, which was not submitted to the
169 reflectance analysis. The collected membrane filters sampled with the Dichotomous and
170 MOUDI samplers were analyzed to the identification of trace elements of mass through
171 X-ray diffraction analysis, mass concentration through gravimetric analysis, and black
172 and organic carbon through reflectance and thermo analysis using a thermal-optical
173 transmittance (TOT) (Sunset Laboratory Inc. – Birch and Cary, 1996). Ion
174 concentrations were evaluated through the ion chromatography analysis of the soluble
175 material collected on the membrane filters (sulphate, nitrate, ammonium, sodium, and

176 chloride). All these samplings were performed on the roof of the main building of the
177 Institute of Astronomy, Geophysics and Atmospheric Sciences of the University of Sao
178 Paulo (IAG-USP) (hereafter also referred as IAG-USP measurement site or simply
179 IAG-USP), which is inside a small green-park (approximately 7.4 km²), with local
180 traffic during the day and surrounded by major roads with intense traffic by light and
181 heavy-duty vehicles (Nogueira et al., 2014). Table 1 lists the aerosol instrumentation
182 deployed roughly at the IAG-USP measurement site. In addition, ambient data from the
183 CETESB's air quality monitoring network and the IAG-USP's climatological station
184 (hereafter also referred as AF-IAG) were also considered for evaluation of numerical
185 simulations. The locations of measurement sites are depicted in Fig. 1 whereas
186 geographic coordinates, urban-suburban classification, and the list of pollutants and
187 meteorological parameters monitored at each site is available in Table 2.

188

189 **2.2. WRF-Chem model**

190 The WRF-Chem model is a fully coupled online meteorological and chemical
191 transport model (Grell et al., 2005), supported by National Center for Atmospheric
192 Research (NCAR) of the USA and several other research institutions around the world.
193 This model is a system of two key components. The WRF-Chem meteorological
194 component, the Weather Research and Forecasting (WRF), is a system configured for
195 both research and operational applications. The dynamical core used in this study is the
196 Advanced Research WRF (ARW). Model's equations into ARW are solved to
197 non-hydrostatic conditions on a fully compressible atmosphere. Further details on the
198 modelling system can be found on the WRF model website (<http://www.wrf-model.org>).
199 On the other hand, the WRF-Chem chemical component treats chemical processes such
200 as dry deposition, gas-phase chemistry, photolysis rates, and aerosols chemistry. A

201 detailed description of the WRF-Chem model can be found on its website
202 (<http://ruc.noaa.gov/wrf/WG11>). Since both meteorological and chemical components
203 are fully coupled, the transport of all chemical species is on-line. The gas-phase
204 chemistry and aerosol modules employed in this study are the Regional Acid Deposition
205 Model, version 2 (RADM2) (Chang et al., 1989) and the Modal Aerosol Dynamics
206 Model for Europe - Secondary Organic Aerosol Model (MADE - SORGAM)
207 (Ackermann et al., 1998; Schell et al., 2001), respectively. The inorganic species
208 included in the RADM2 mechanism are 14 stable species, 4 reactive intermediates, and
209 3 abundant stable species (oxygen, nitrogen and water). Atmospheric organic chemistry
210 is represented by 26 stable species and 16 peroxy radicals. The RADM2 mechanism
211 represents organic chemistry through a reactivity aggregated molecular approach
212 (Middleton et al., 1990). Similar organic compounds are grouped together in a limited
213 number of model groups through the use of reactivity weighting. The aggregation
214 factors for the most emitted VOCs are given in Middleton et al. (1990).

215 On the other hand, the most important process for the formation of secondary
216 aerosol particles is the homogeneous nucleation in the sulfuric acid-water system. It is
217 parameterized in MADE, following the method of Kulmala et al. (1998). Aerosol
218 growth by condensation occurs in two steps: the production of condensable material
219 (vapor) by the reaction of chemical precursors, and the condensation and evaporation of
220 ambient volatile species on aerosols. The inorganic chemistry system, based on the
221 Model for an Aerosol Reacting System (MARS) (Saxena et al., 1986) and its
222 modifications by Binkowski and Shankar (1995), calculates the chemical composition
223 of a sulphate-nitrate-ammonium-water aerosol according to equilibrium
224 thermodynamics. The organic aerosol chemistry is based on the SORGAM, which
225 assumes that SOA compounds interact and form a quasi-ideal solution (Grell et al.,

226 2005). The SOA formation in SORGAM follows the two-product approach (Odum et
227 al., 1996) where the oxidation of hydrocarbons produces two types of modelled
228 semivolatile compounds that are partitioned between the gas and particle phases after
229 considering the absorptive partitioning theory (Pankow, 1994a; b). The primary organic
230 aerosol (POA) in MADE is calculated from the primary anthropogenic emission of OC.
231 Then, one may calculate the predicted OC concentration from the sum of both SOA and
232 POA. The concurrent organic matter (OM) can be obtained from the OC concentration
233 by application of a conversion factor. Brown et al. (2013) showed that the average
234 OM:OC ratio was 1.54 (with a standard deviation of 0.2) for sites with low amount of
235 secondary aerosol formation. It is important to note that this ratio can change from one
236 place to another. In areas impacted by biomass burning the ratio can be higher. Gorin et
237 al. (2006) assumed a ratio of 1.6 for the conversion from OC to OM over an area that
238 experiences a significant wood smoke influence.

239

240 **2.2.1. Model configuration**

241 WRF-Chem version 3.5 was configured with three nested grid cells: coarse (75
242 km), intermediate (15 km) and fine (3 km). The coarse grid cell covered a big region of
243 Brazil and also of the Atlantic Ocean. The intermediate grid covered the southeast
244 Brazil while the fine grid cell covered barely the SPMA and metropolitan areas nearest
245 to it. Fig. 1 shows the arrangement of measurement sites and topography in the
246 downtown area of the 3-km modelling domain. The initial and boundary meteorological
247 conditions are from the National Center for Environmental Prediction's Final
248 Operational Global Analysis with 1° of grid spacing, 26 vertical levels and are available
249 every six hours: 00, 06, 12 and 18 UTC (<http://rda.ucar.edu/datasets/ds083.2/>). The
250 initial and boundary chemical conditions for representing gases and aerosols

251 background concentration were obtained from the Model for Ozone and Related
252 chemical Tracers, version 4 (MOZART-4; Emmons et al., 2010). This model was driven
253 by meteorological inputs from the Goddard Earth Observing System Model, version 5 at
254 a horizontal resolution of $1.9^{\circ} \times 2.5^{\circ}$, 56 vertical levels that are also available every six
255 hours. Table 3 lists the WRF-Chem configuration options employed by this study.

256 WRF-Chem simulation with coupled primary aerosol (dust, sea salt and
257 anthropogenic) and gas (biogenic and anthropogenic) emission modules, together with
258 the direct effect of aerosol particles turned on, is performed as the control simulation in
259 order to evaluate the model performance (hereafter referred to as Case_0). For
260 secondary aerosols, a simulation scenario (Case_1) with biogenic and anthropogenic
261 gases emission is performed to evaluate its formation potential. An additional
262 simulation (Case_2) is also performed to evaluate the impact of aerosols on ozone
263 photochemistry. Notation and description of simulations are listed in Table 4. The first
264 seven days of each simulation were not analyzed and used for model spin-up.

265

266 **2.3. Emissions**

267 **2.3.1. Anthropogenic emissions**

268 Because on-road vehicles are the most important sources of air pollution in
269 southeast Brazil's metropolitan areas, particularly in SPMA where, according to
270 CETESB, more than 80% of pollutant emissions are generated by vehicular emissions;
271 the anthropogenic emissions of trace gases and particles in both 3 and 15 km modelling
272 domains were considered to include emissions only coming from on-road vehicles
273 through the use of a vehicular emission model developed by the IAG-USP's Laboratory
274 of Atmospheric Processes (LAPAt). Basically, this model considers the number of
275 vehicles, vehicular emission factors, and average driving kilometers for vehicle per day

276 as basic parameters for the calculation of exhaust emissions considering different
277 vehicle types (light-duty vehicles, heavy-duty vehicles, and motorcycles) and different
278 fuel types (ethanol, gasohol, combination of any proportion of gasohol and ethanol, and
279 diesel) according to CETESB (2012). The details of this model are available in Andrade
280 et al. (2015). In the case of VOCs, there are other two relevant emissions (fuel transfer
281 and evaporative processes) associated with the vehicles, besides the exhaust emissions.
282 Because of the complexities in the spatial representation due to a numerous factors such
283 as emissions at service stations, such emission sources are assumed to be emitted by
284 exhaust of vehicles for the sake of simplicity. The vehicular fleet and intensity of use
285 datasets are provided by the National Department of Traffic (DENATRAN) and the Sao
286 Paulo Transporte (SPTrans), respectively. Emission factors for road vehicles for most
287 pollutants were considered from previous studies performed inside road tunnels (i.e.
288 Janio Quadros, referred as JQ tunnel, and the tunnel 3 of the Rodoanel Mario Covas that
289 is referred hereafter as RA tunnel) located within the SPMA (Pérez-Martínez et al.,
290 2014; Nogueira et al., 2014). However, emission factors for VOCs are considered from
291 dynamometer protocols (CETESB, 2010). VOCs and PM speciation profiles used by
292 gas-phase and aerosol chemical modules were also obtained from NUANCE-SPS
293 experimental campaigns performed in 2011 (tunnel measurements) and 2012 (ambient
294 data). It is important to note that due to the lack of information on vehicular emission
295 factors and intensity of use for most of the other metropolitan areas inside both
296 modelling domains (e.g. the Campinas Metropolitan Area, which is shown by the
297 second largest grey stain in Fig. 2), the calculation of vehicular emissions for these
298 urban areas was carried out on the basis of the parameters found for the SPMA. The
299 number of vehicles in any modelling domain is calculated from the sum of the number
300 of vehicles in each one of the main urban areas inside the modelling domain in question.

301 Spatial distribution of emissions for the 3 km modelling domain resolution was
302 based on road density products compiled by the OpenStreetMap project and extracted
303 from the Geofabrik's free download server (<http://download.geofabrik.de>). Urban areas
304 were assumed to allocate high emissions since these concentrate a road density greater
305 than other areas. In the case of the 15 km modelling domain, emissions are based on
306 night-time lights data from the Defense Meteorological Satellite Program
307 (<http://ngdc.noaa.gov/eog/dmsp/downloadV4composites.html>). These images are 30 arc
308 second grids, spanning from -180° to $+180^{\circ}$ longitude and -65° to $+75^{\circ}$ latitude and
309 contain the lights from cities, towns and other sites with persistent lighting, including
310 gas flares. Cleaned up night-time light points with no ephemeral events such as forest
311 fires are used to allocate emissions. To estimate the number of vehicles in each grid
312 point of both domains, the sum of individual intensities at each point (i.e. total road
313 length for the 3 km modelling domain and night-time light for the 15 km modelling
314 domain) is firstly normalized by the total fleet, and then distributed uniformly using the
315 total fleet distribution so that emissions in urban areas are mainly represented by
316 emissions coming from their vehicles. Furthermore, due to the complexity involved in
317 describing the temporal variation of emissions at each grid point, median values for
318 vehicular traffic obtained from measurements inside the JQ and RA tunnels
319 (Pérez-Martínez et al., 2014) were used for distributing the emissions during the day in
320 both domains. This approximation followed the approach used by Fast et al. (2006)
321 where emission profiles were calculated from median diurnal variations on weekdays
322 and weekends. We have applied the same constant diurnal cycle at all grid points where
323 emissions have values greater than zero. VOC and PM emission profiles were assumed
324 to be the same as for CO and NO_x emission profiles since these pollutants are also
325 characteristic tracers of emissions of light-duty and heavy-duty vehicles, respectively.

326 Fig. 2 shows the maximum hourly emission rates for aromatic VOCs in the 3 km
327 modelling domain. Anthropogenic emissions were not considered in the 75 km
328 modelling domain.

329 The Another Assimilation System for WRF-Chem (AAS4WRF) chemical
330 emissions pre-processor developed by the Latin American Observatory (OLE2; Muñoz
331 et al., 2010; 2012) was used to scale emission rates on WRF curvilinear coordinates.
332 AAS4WRF is appropriate to write chemical emission rates from both surface and
333 elevated sources in the proper WRF data file format, providing an alternative tailored
334 way to assimilate emissions to WRF-Chem. The method is explained in the OLE2 Wiki
335 pages in detail (http://www.cmc.org.ve/mediawiki/index.php?title=Calidad_de_Aire).

336

337 **2.3.2. Other emissions**

338 Biogenic emissions are calculated online based on the Guenther scheme
339 (Guenther et al., 1993; 1994). The Guenther biogenic emissions model calculates the
340 emission rates using temperature, photo-synthetically active radiation flux and land-use
341 data as the U.S. Geological Survey (USGS) land-use cover system classification if
342 coupled with the WRF model. However, as indicated in the WRF-Chem emissions
343 guide (http://ruc.noaa.gov/wrf/WG11/Emission_guide.pdf), several key chemical
344 species would have been representing relatively low emission rates because of the
345 limited vegetation types in the simulation, and thus their impacts are anticipated to be
346 much lower than those from vehicular emissions.

347 Dust and sea salt emissions are calculated online following the works of Ginoux
348 et al. (2001) and Gong (2003), respectively. The calculation of Ginoux et al. (2001) for
349 the uplifting of dust particles is based on the surface wind speed, wetness and
350 information on soil characteristics. The model then solves the continuity equation

351 including the emission, chemistry, advection, convection, diffusion, dry deposition, and
352 wet deposition of each species. The parameterization of sea salt aerosol source function
353 of Gong (2003) is an extended parameterization of Monahan et al. (1986), which scales
354 the generation of marine aerosols from mechanical disruption of wave crests by the
355 wind and sea surface covered by whitecaps.

356

357 **3. Results and discussion**

358 **3.1. Characterization of meteorological conditions**

359 In order to study and understand the spatial and temporal variability of
360 atmospheric aerosols, O₃, and other pollutants (i.e. CO, NO_x) during the study period, it
361 was first necessary to analyze the behavior of main meteorological systems acting on
362 the atmospheric environment of the SPMA and surrounding areas.

363 According to the monthly climate reports from the IAG-USP's Climate Research
364 Group (GrEC), the observed precipitation rates were lower than the climatological value
365 in SPMA (anomaly of -38.6 mm) and larger part of the Sao Paulo State during August
366 2012. Negative anomalies on the precipitation were caused by the intensification of the
367 South Atlantic Subtropical High (SASH). These conditions established an easterly wind
368 anomaly pattern at the 850 hPa level. Conditions were unfavorable for relative humidity
369 coming from the Amazon due to the Low Level Jet (LLJ) and less intense Alisian winds
370 in the Tropical Atlantic (GrEC, 2012a). However, the action of frontal systems favored
371 the rain accumulation in September 2012, mainly in western Sao Paulo State where the
372 greater positive amount of anomalies was observed. Precipitation events were
373 predominantly observed during the second half of the month. In this case, the wind
374 pattern showed an opposite configuration to that observed in August 2012 as a result of
375 the weakening of the SASH (GrEC, 2012b). The IAG-USP's climatological station

376 recorded an accumulated precipitation of about 1.3 mm on three days of occurrence (28
377 August, 30 August and 4 September 2012) and an easterly wind pattern with a median
378 intensity of 2 m s^{-1} during the period between 07 August and 06 September 2012. Fig. 3
379 shows the hourly accumulated precipitation and relative humidity observed at the
380 IAG-USP's climatological station.

381

382 **3.2. Analysis of aerosol species**

383 Aerosol analysis included species such as organic carbon (OC), elemental
384 carbon (EC), sulphate, nitrate, ammonium, sodium and chloride in addition to other
385 elemental constituent of PM. All the samplings for these species were performed at
386 IAG-USP. Results showed that the major contributors to the concentration of fine
387 particles are OM (55.7%; OM:OC ratio of 1.5 found by Brito et al. (2013)) and EC
388 (15%), followed by sulphate (2.9%), ammonium (2.1%), sodium (1.9%), nitrate (0.5%)
389 and chloride (0.3%). The remaining mass (21.6%) is calculated by determining of the
390 difference between the total mass of $\text{PM}_{2.5}$ (from the gravimetric analysis) and the sum
391 of the masses of 7 individual compounds, as noted above. Part of this remaining mass is
392 related to the water content of aerosols (Andrade et al., 2012).

393 On the other hand, $\text{PM}_{2.5}$, PM_{10} and size distribution of particles measured at
394 IAG-USP show that the study period was characterized by a reduction in the
395 concentrations up to the end of August 2012 when their minimum values were achieved.
396 This reduction was related to the action of a semi-stationary front between the coasts of
397 Sao Paulo and Parana States. After the passage of this system, aerosol concentrations
398 have significantly increased what could be related to an increase in relative humidity

399 once the SASH system is moved away from the continent, as well as the transport of
400 aerosol particles produced by forest fires in the central-west region of Brazil and the Sao
401 Paulo State. Several studies have shown the contribution of forest fires on the
402 atmospheric aerosol concentrations in SPMA (Vieira-Filho et al., 2013; Vasconcellos et
403 al., 2010). One way to qualitatively evaluate the contribution of forest fires on aerosol
404 concentrations is by using the air mass trajectories. The Hybrid Single-Particle
405 Lagrangian Integrated Trajectory (HYSPLIT) model (Draxler and Hess, 1998) was used
406 to calculate backward trajectories of air masses in order to identify atmospheric
407 transport of air mass from forest fire areas. Fig. 4 shows the three-day backward
408 trajectories of air masses starting at IAG-USP for the days 9 and 31 August and 5
409 September, when increases in the OC and EC concentrations were observed at
410 IAG-USP. The pink markers on the map represent the observed fire locations during the
411 study period considering different satellite products (GOES, AQUA, TERRA, NOAA).

412 Fig. 5 shows the concentration of OC, EC and some species of PM_{2.5} during the
413 study period at IAG-USP. We can observe eleven exceedances of PM_{2.5} concentration
414 with respect to the air quality standard of 25 µg m⁻³ (see grey line in Fig. 5a) established
415 by the World Health Organization (WHO). These exceedances have mainly occurred at
416 the beginning and at the end of the study period when an increase in the concentrations
417 of OC and EC were observed. The increasing organic matter could be associated to
418 traffic incidents which may raise the emissions, which in case of less favorable
419 meteorological conditions (e.g. lower height of lower planetary boundary layer, PBL, or
420 slow transport of air pollutants) may have led to a more efficient formation of secondary
421 particles. Castanho and Artaxo (2001) analyzed the behavior of the aerosol composition
422 in SPMA and showed the increase in the concentration of inorganic and organic material
423 in the winter season compared to the summer season, explaining this behavior with the

424 meteorological characteristics: dry conditions with low height inversion layer in the
425 wintertime and a rainy summer.

426 Size distributions of aerosol mass indicate that the majority of sulphate,
427 ammonium and PM₁₀ mass concentration is distributed in the size range with diameters
428 between 0.1 and 1 µm, commonly known as accumulation mode particles (Kumar et al.,
429 2010). In the cases of nitrate, sodium, and chloride, most part of mass was concentrated
430 in particles with diameters greater than 1 µm.

431 432 **3.3. Comparison of baseline simulation with observations**

433 All the numerical results presented in this section, for the purpose of comparison
434 with the measurements, were obtained from the baseline simulation (Case_0). The
435 predicted temperature, humidity, and 10-m wind speed and direction have been
436 compared to measurements from the AF-IAG and INT measurement sites. Overall, the
437 model captured the diurnal variation of temperature, relative humidity, and wind
438 directions reasonably well. However, the predicted wind speeds were higher than the
439 observed values. To evaluate the model performance in solving the meteorology and
440 chemical species, we computed the statistics correlation coefficient (R), mean bias
441 (MB), mean fractional bias (MFB), mean fractional error (MFE), and root mean square
442 error UB (RMSE_{UB}). The definitions of these statistics are given in the Appendix. Fig. 6
443 shows the predicted average of 10-m wind vectors and 2-m temperature for the whole
444 study period in the 3 km modelling domain. Blue dots represent the locations of
445 AF-IAG and INT sites, while the numbers in cyan indicate the observed average
446 temperatures (i.e. 17.7 °C at AF-IAG and 17.8 °C at INT). On an average, the predicted
447 wind direction was easterly in SPMA, which has somewhat affected the spatial
448 distribution of aerosol particles as examined later in this section. Likewise, the statistics

18

449 used to quantify the model performance in the representation of PM concentration show
450 that, in general, most of prediction-observation pairs present good correlation
451 coefficients, mainly those for PM₁₀, but with negative biases and standard deviations
452 lower than those for observations (see Fig. 10). Table 5 summarizes the performance
453 statistics used in this study showing comparisons between WRF-Chem predictions and
454 observations. The evaluation of WRF-Chem predictions for meteorology and chemical
455 species on a site-by-site basis is presented in the sections 1 and 2, respectively, of the
456 supplementary material. Figs. 7, 8 and 9 show the observed and predicted temporal
457 variations of PM_{2.5}, PM₁₀ and O₃ concentrations at 3, 10 and 6 sites in the SPMA,
458 respectively, with some measurement sites sharing the same grid point for comparisons
459 due to the geographical proximity (e.g. the sites IAG-USP and IPEN-USP both
460 separated around 900 m from each other). These figures suggest that predicted
461 concentrations did not present any significant spatial variation in the downtown SPMA
462 and were generally underestimated when compared to measurements. This under
463 prediction could be associated with an underestimation on the vehicular emissions as
464 well as other emission sources (e.g. emissions coming from industry) that are
465 disregarded in this study, in addition to predicted surface winds more intense than those
466 observed, leading to a dilution of aerosol particles in the SPMA. The high
467 concentrations of PM_{2.5} and PM₁₀ observed at the beginning and at the end of the study
468 period, whose variability and trends were reasonably well captured by the model, could
469 be related with the emission of high aerosol loadings due to traffic incidents as well as
470 the establishment of lower PBL heights, commonly observed under post-frontal
471 situations. The results for this simulation (Case_0) show that overall the predicted PBL
472 heights (not shown here) have a regular diurnal variation in the downtown SPMA with
473 averaged daily values around 500 m at both the beginning and the end, and of up to 700

474 m in the middle of the study period, when lower concentrations of aerosols were
475 observed.

476 Figures 11-13 show the predicted average surface distribution of $PM_{2.5}$, PM_{10} and
477 $PM_{2.5}:PM_{10}$ ratio for the 3 km modelling domain, respectively. Red dots and cyan
478 numbers represent the locations and the observed mean PM concentrations (or mean PM
479 concentration ratios) at the measurement sites, respectively. Major contributions of
480 $PM_{2.5}$ on the total PM_{10} concentration were observed mainly over offshore continental
481 areas (see Fig. 13). High $PM_{2.5}:PM_{10}$ concentration ratios would be firstly associated
482 with the transportation of fine particles and gases from upwind regions (see Fig. 6),
483 followed by a production of fine particles from biogenic emissions. Additional
484 comparisons between the observed and predicted concentrations of OC and EC at
485 IAG-USP (the only site with measurements of OC and EC) are shown in Fig. 14. As it
486 has been pointed out in the section 2 of the supplementary material, under predicted OC
487 concentrations could be associated, among others (e.g., underestimation of POA
488 emissions, inaccurate meteorological predictions), with an underestimation of SOA,
489 probably due to the absence of oxidation of monoterpenes and a limited treatment of
490 anthropogenic VOCs oxidation in the RADM2 mechanism, as discussed by Tuccella et
491 al. (2012). The SORGAM aerosol module considers the formation of anthropogenic
492 SOAs from the oxidation of alkane, alkene and aromatic VOCs as well as the biogenic
493 SOA formation from the oxidation of alpha-pinene, limonene and isoprene VOCs.
494 Recent studies coupling non-traditional SOA models (volatility basis set approaches) in
495 WRF-Chem show improvements in the predicted SOA concentrations, although these
496 are still lower than those observed (e.g. Li et al., 2011b; Ahmadov et al., 2012;
497 Shrivastava et al., 2013).

498 On the other hand, measurements of mass size distribution were also made with
499 a MOUDI impactor at IAG-USP, following the protocol describe in Miranda and
500 Andrade (2005). Constituents of aerosol were subsequently determined by X-Ray
501 fluorescence analysis and ion chromatography analysis. As previously indicated in this
502 section, the main identified species are SO₄, NO₃, NH₄, Na and Cl. The observed
503 average aerosol composition is derived using measurements from both MOUDI
504 impactor and SUNSET analyzer. To perform the comparisons of mass size distribution,
505 we adequately joined the MOUDI bin sizes according to the three modes used by the
506 MADE aerosol module: Aitken (<0.1 μm), accumulation (0.1-1 μm) and coarse (>1
507 μm). The observed and predicted aerosol mass size distributions averaged over the same
508 sampling time period (16 days along the study period) are shown in Fig. 15. Over the
509 downtown SPMA, both the observed and predicted fine particles from accumulation
510 mode account for majority of the total PM_{2.5} mass. Since the formation-growth
511 processes of aerosols in question are explicitly treated in the Aitken and accumulation
512 modes, the predicted concentrations for particles larger than 1 μm are assumed to be
513 zero. In this case, the mass of particles larger than 1 μm is allocated to the PM₁₀ aerosol
514 variable (see Fig. 15). The comparison between the observed and predicted average
515 contributions for the main identified aerosol constituents at IAG-USP is shown in Fig.
516 16. Both the observed and predicted OC and EC make up the largest fraction of PM_{2.5}
517 mass with contributions of 55 and 40%, respectively. In addition, it was found that the
518 predicted SOA concentrations contribute 17% of the predicted total OC concentration at
519 this measurement site. Various global and regional scale SOA simulations have been
520 conducted using mass-based yield and partitioning coefficients, but they have
521 underestimated the SOA concentrations by roughly an order of magnitude, especially
522 over urban regions (Matsui et al., 2014). Using the same SOA formation approach

523 employed by this study and a conversion factor of 1.6 to convert the emissions of OC to
524 OM, Tuccella et al. (2012) found simulated SOA:OM ratios in the 5-40% range against
525 the observed range of 50-80%. Although the predicted average PM_{2.5} concentration
526 (14.48 µg m⁻³) was lower than observed (22.32 µg m⁻³), the mean aerosol chemical
527 composition was reasonably well represented by the model (see Fig. 16).

528 **3.4. Contribution of dust-sea salt and coarse anthropogenic aerosols to PM** 529 **concentration**

530 The evaluation of the contribution of dust and sea salt aerosols on PM₁₀
531 concentration is performed from the sum of their concentrations divided by the PM₁₀
532 concentration. The simulated average ratio between dust-sea salt aerosols and the total
533 PM₁₀ mass concentration is shown in Fig. 17b. High concentration ratios have been
534 observed over the ocean where sea salt emissions are by far the most important aerosols
535 source. Unlike high concentration ratios over the ocean, lower concentration ratios are
536 observed over the continent far away from the coast. In this region, the main sources of
537 atmospheric aerosols would be the emission of primary biological aerosol, SOA formed
538 from the emission of biogenic volatile organic compounds (BVOCs), and forest fires.
539 However, particles could also be transported from remote areas. In addition, we can also
540 observe that dust and sea salt aerosols have a contribution between 40 and 50% of the
541 total PM₁₀ concentration in the downtown SPMA. Furthermore, it is possible to estimate
542 the contribution of all the other PM₁₀ (i.e., the coarse anthropogenic aerosol) to the total
543 PM₁₀ mass concentration. It may be directly calculated from the model or estimated
544 from the Figs. 13 and 17b once the sum of concentrations of PM_{2.5}, dust and sea salt,
545 and coarse anthropogenic aerosol represents 100% of the total PM₁₀ mass concentration.
546 For example, we found that the coarse anthropogenic aerosol represents around 10% of
547 PM₁₀ in the downtown SPMA.

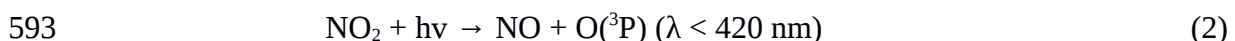
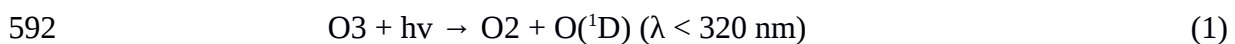
548 **3.5. Evaluation of secondary aerosol formation**

549 As described in Section 2.1, aerosol module employed by this study
550 (MADE/SORGAM) includes the homogeneous nucleation in the sulphuric acid-water
551 system. The sulphuric acid is the most significant condensable molecule formed in the
552 atmosphere, which has also been long recognised as the most important molecule from
553 the point of view of the nucleation of new particles (Jenkin and Clemitshaw, 2000;
554 Seinfeld and Pandis, 2006). However, for the SPMA, the importance of SOA formed
555 from the anthropogenic emission of fuel used by the transport sector was noted (Salvo
556 and Geiger, 2014). According to the official emission inventory developed by the Sao
557 Paulo Environmental Protection Agency (CETESB, 2013), the SOA explains 51% of the
558 fine particle mass concentration, with the vehicular emission being its main source. The
559 subsequent growth processes involve aerosol growth by condensation of condensable
560 material onto existing particles, and by coagulation of particles to form larger particles
561 (Kumar et al., 2011; 2014). For example, particles in the accumulation mode emerge
562 through coagulation of particles from the Aitken mode (Kumar et al., 2011). It is
563 important to emphasize that the boundaries were updated with gas and aerosol
564 background concentrations coming from the 15 km modelling domain during the whole
565 simulation period. Thereafter, the impact of vehicular emissions on the formation of fine
566 particles was calculated from the predicted $PM_{2.5}$ concentration considering an emission
567 scenario (Case_1) in which only emission of gases from vehicles and vegetation are
568 taken into account to be emitted to the atmosphere from the surface. The predicted
569 average $PM_{2.5}(\text{Case}_1):PM_{2.5}(\text{Case}_0)$ ratio is shown in Fig. 17a. A contribution
570 between 20 and 30% in the predicted baseline $PM_{2.5}$ concentration in downtown SPMA
571 is found to correspond to the fine particles formation and transportation processes.
572 Higher concentration ratios over the SPMA surroundings (30-50%) could be associated

573 with more efficient biogenic emissions. Overall, it is observed that the formation
574 efficiency increases towards the northwest from the ocean. Deep red areas in Fig. 17a
575 could also be associated with the transportation of fine particles and gases from other
576 regions, in addition to having a more efficient production of fine particles from biogenic
577 emissions. For example, given the distribution of winds in Fig. 6, the northern boundary
578 could represent the main source of particles and gases over this part of the simulation
579 domain. Additionally, the comparison between the predicted and observed OC and EC
580 concentrations at IAG-USP shown in Fig. 14 includes the Case_1 simulation in which
581 only emission of primary gases is taken into account in the assessment of fine particles
582 formation. The concentration peaks observed at the beginning and at the end of the
583 study period may be associated with the transport of aerosol particles from both biomass
584 and fossil fuel burning areas (see Fig. 4). Considering the Case_1 simulation, we can
585 observe very low concentrations for EC (mean concentration of $0.01 \mu\text{g m}^{-3}$), as
586 expected. This is because these particles are not produced by photochemical processes
587 in the atmosphere, but associated mainly with the diesel exhaust.

588 **3.6. Aerosol impact on O₃ photochemistry**

589 Ozone photochemistry production mainly depends on the two key photolysis
590 rates, as shown in Eqs. (1) and (2), i.e., shortwave radiation able to reach the surface to
591 break molecules of O₃ and NO₂.



594 Therefore, the impact of aerosols on O₃ photochemistry has been evaluated from
595 the impact of aerosols on downward shortwave radiation. Attenuation (scattering and

596 absorption) of downward shortwave radiation by aerosols may substantially modify the
597 photolysis rates, and thereby affecting the ozone photochemistry production.

598 The average percentage change in surface O₃ concentrations at 16:00 h (local
599 time) with and without the aerosol-radiation feedback module turned on are shown Fig.
600 17c. Overall O₃ is destroyed or formed (incoming transport from other regions) in small
601 quantities between -1 and +1% in relation to its total concentration. In addition, it was
602 observed that the surface O₃ concentration decreased by around 2% in the downtown
603 SPMA. Li et al. (2011a) found that the impact of aerosols on O₃ formation in Mexico
604 City was most pronounced in the morning with the O₃ reduction of 5-20%, but the
605 reduction is less than 5% in the afternoon. Low reductions in the O₃ concentration in the
606 downtown SPMA compared to results from other studies may be explained by the lower
607 predicted PM₁₀ concentrations, which can lead to a minor attenuation of the incoming
608 solar radiation. Simulated mean downward shortwave fluxes at ground surface (not
609 shown) were up to 5% higher for the Case_2 than for the Case_0 during the afternoon.
610 The inclusion of the direct effect of aerosol particles was found to have small reductions
611 in the surface temperature (changes by around 2%), presumably due to an increase in
612 the number of atmospheric processes involving downward longwave fluxes over this
613 area. Forkel et al. (2012) found an underestimation of predicted downward longwave
614 radiation over the southern Baltic Sea when the direct effect of aerosol particles was
615 neglected. Despite the highly non-linear behavior of tropospheric O₃, the reduction in
616 the predicted O₃ concentrations indicates a high efficiency of aerosols to attenuate the
617 downward shortwave radiation, what is plausible once it was found that low PM₁₀
618 concentrations have a capability to reduce ground level O₃ concentrations in a few ppb.

619 **4. Summary and conclusions**

620 The WRF-Chem community model has been used to evaluate the impact of
621 vehicular emissions on the fine particles formation in the SPMA. Three thirty-one day
622 simulations, covering a period from 7 August to 6 September 2012, have been
623 performed. The aims were to evaluate the impact of fine particles formation (both
624 inorganic and SOA) from gases emitted by road vehicles as well as the aerosol impacts
625 on the ozone formation photochemistry. The results were compared with the
626 measurements available from the NUANCE-SPS project.

627 The predicted temporal variations of meteorology, $PM_{2.5}$, PM_{10} and O_3 were
628 found to agree well with the measurements at most of the sites during the entire
629 simulation period. However, the predicted concentrations of $PM_{2.5}$, PM_{10} and O_3 (but in
630 minor intensity) were lower than the observed values. This difference could be
631 associated with an underestimation of the vehicular emissions and other emission
632 sources such as industry, heating and cooking, which are not considered in this study.
633 Wind speed and direction played an important role in the distribution of fine particles
634 over the simulation domain. Backward trajectories analysis suggested that aerosol
635 particles from biomass burning were transported to SPMA, impacting on the PM
636 concentration over this region.

637 The baseline simulation (Case_0) showed that dust and sea salt aerosols made a
638 contribution between 40 and 50% of the total PM_{10} concentration in the downtown
639 SPMA. On the other hand, the Case_1, which represents simulations with gaseous
640 emissions only, indicates that the emissions of primary gases coming mainly from
641 vehicles have a potential to form new particles between 20 and 30% in relation to the
642 baseline $PM_{2.5}$ concentration found in the downtown SPMA. Finally, the Case_2, which
643 represents simulations with aerosol-radiation feedback turned on, reveals a reduction in

644 the surface O₃ concentration by around 2% in the afternoon (16:00 h; local time) when
645 the aerosol-radiation feedback is taken into account.

646 This study provides a first step to understand the impact of vehicular emissions
647 on the secondary particles formation in the SPMA. Nevertheless, more experimental
648 campaigns are recommended for future work in order to characterize aerosols in
649 ambient air and to improve their emission estimates so that a better understanding of
650 physical and chemical properties and their formation can be established. This study also
651 evaluates the importance of the VOCs in the formation of not only O₃ but also of fine
652 particles. These compounds play an important role concerning health impacts and
653 climate change, and the control of their concentrations requires the description of their
654 formation mechanisms.

655 **Appendix**

656 The statistics used in this study are defined as follows:

657 1. Mean bias (MB)

$$MB = \frac{1}{n} \sum_{i=1}^n (M_i - O_i)$$

658

659 2. Mean fractional bias (MFB)

$$MFB = \frac{1}{n} \sum_{i=1}^n \frac{2(M_i - O_i)}{M_i + O_i} 100\%$$

660

661 3. Mean fractional error (MFE)

$$MFE = \frac{1}{n} \sum_{i=1}^n \frac{2|M_i - O_i|}{M_i + O_i} 100\%$$

662

663 4. Root mean square error UB (RMSE_{UB})

$$\text{RMSE}_{\text{UB}} = \sqrt{\frac{1}{n} \sum_{i=1}^n [(M_i - \bar{M}) - (O_i - \bar{O})]^2}$$

664

665 5. Correlation coefficient (R)

$$r = \frac{\sum_{i=1}^n (M_i - \bar{M}) * (O_i - \bar{O})}{\sqrt{\sum_{i=1}^n (M_i - \bar{M})^2} \sqrt{\sum_{i=1}^n (O_i - \bar{O})^2}}$$

666

667 Where

668 $\bar{O} = \frac{1}{n} \sum_{i=1}^n O_i$ and $\bar{M} = \frac{1}{n} \sum_{i=1}^n M_i$ are the average values of the individual observed and

669 predicted values, O_i and M_i , respectively. “n” is the number of observations.

670

671 5. Acknowledgments

672 Prashant Kumar, Angel Vara-Vela and Maria de Fatima Andrade thank the
673 University of Surrey's International Relations Office for the Santander Postgraduate
674 Mobility Award that helped Angel Vara to visit University of Surrey, UK, and develop
675 this research article collaboratively. The authors from Universities of Surrey and Sao
676 Paulo also acknowledge the collaborative funding received through the University
677 Global Partnership Network (UGPN) to the project titled “*Emissions And Role Of Fine*
678 *Aerosol Particles In Formation Of Clouds and Precipitation (eRAIN) - A demonstration*
679 *study for the megacity, São Paulo*” for supporting this research work. Maria de Fatima

680 Andrade and Angel Vara-Vela acknowledged funding from the Coordination for the
681 Improvement of Higher Education Personnel (CAPES) and Research Foundation of the
682 State of Sao Paulo (FAPESP, project 2008/58104-8) that allowed the experimental
683 campaigns. The authors also thank the WRF-Chem developers, the NOAA's National
684 Geophysical Data Center, the NCAR's Data Support Section and Atmospheric
685 Chemistry Division, the Latin American Observatory (OLE2), the Sao Paulo
686 Environmental Protection Agency (CETESB), the OpenStreetMap Data Extracts, and
687 the NCAR Command Language (NCL) software for providing the tools and datasets
688 used in this research.

689

690 **6. References**

- 691 Ackermann, I. J., Hass, H., Memmesheimer, M., Ebel, A., Binkowski, F. S., and
692 Shankar, U.: Modal aerosol dynamics model for Europe: development and
693 first applications, *Atmos. Environ.*, 32, 2981-2999, 1998.
- 694 Ahmadov, R., McKeen, S. A., Robinson, A. L., Bahreini, R., Middlebrook, A. M., de
695 Gouw, J. A., Meagher, J., Hsie, E. Y., Edgerton, E., Shaw, S., and Trainer,
696 M.: A volatility basis set model for summertime secondary organic
697 aerosols over the eastern United States in 2006, *Journal of Geophysical*
698 *Research*, 117, D06301, doi:10.1029/2011JD016831, 2012.
- 699 Albuquerque, T. T. A., Andrade, M. F., and Ynoue, R. Y.: Characterization of
700 atmospheric aerosols in the city of Sao Paulo, Brazil: comparisons between
701 polluted and unpolluted periods, *Water Air Soil Pollution*, 195, 201-213, 2011.
- 702 Anderson, L.: Ethanol fuel use in Brazil: air quality impacts, *Energy Environ. Sci.*, 2,
703 1015-1037, 2009.

704 Andrade, M. F., Ynoue, R. Y., Freitas, E. D., Todesco, E., Vara-Vela, A., Ibarra, S.,
705 Martins, L. D., Martins, J. A., Carvalho, V. S. B.: Air quality forecasting system
706 for Southeastern Brazil, *Front. Environ. Sci.*, 3, 1-14, 2015.

707 Andrade, M. F., Fornaro, A., Miranda, R. M., Kerr, A., Oyama, B., Andre, P. A., and
708 Saldiva, P.: Vehicle emissions and PM_{2.5} mass concentrations in six
709 Brazilian cities, *Air Quality, Atmosphere and Health*, 5, 79-88, 2012.

710 Binkowski, F. S. and Shankar, U.: The regional particulate matter model, 1. Mode
711 description and preliminary results, *Journal of Geophysical Research*, 100,
712 26191-26209, 1995.

713 Birch, M. E. and Cary, R. A.: Elemental carbon-based method for occupational
714 monitoring of particulate diesel exhaust: methodology and exposure issues,
715 *Aerosol Science and Technology*, 25, 221-241, 1996.

716 Brito, J., Rizzo, L. V., Herckes, P., Vasconcellos, P. C., Caumo, S. E. S., Fornaro,
717 A., Ynoue, R. Y., Artaxo, P., and Andrade, M. F.: Physical-chemical
718 characterisation of the particulate matter inside two road tunnels in the Sao
719 Paulo Metropolitan Area, *Atmos. Chem. Phys.*, 13, 12199-12213, 2013.

720 Brown, S. G., Lee, T., Roberts, P. T., and Collett, J. L. Jr.: Variations in the OM/OC ratio
721 of urban organic aerosol next to a major roadway, *J. Air & Waste Manag. Assoc.*,
722 63(12), 1422-1433, 2013.

723 Carvalho, V. S. B., Freitas, E. D., Martins, L. D., Martins, J. A., Mazzoli, C. R., and
724 Andrade, M. F.: Air quality status and trends over the Metropolitan Area of
725 Sao Paulo, Brazil as a result of emission control policies, *Environmental
726 Science & Policy*, 47, 68-79, 2015.

727 Castanho, A. D. A. and Artaxo, P.: Sao Paulo aerosol source apportionment for
728 wintertime and summertime, *Atmos. Environ.*, 35, 4889-4902, 2001.

729 Costa, R. C. and Sodré, J. R.: Hydrous ethanol vs. gasoline-ethanol blend: Engine
730 performance and emissions, *Fuel*, 89, 287-293, 2010.

731 CETESB-Companhia de Tecnologia de Saneamento Ambiental. Relatório Anual de
732 Qualidade do Ar no Estado de São Paulo 2012, São Paulo, 2013.

733 CETESB-Companhia de Tecnologia de Saneamento Ambiental. Emissões
734 veiculares no Estado de São Paulo 2011, São Paulo, 2012.

735 CETESB-Companhia de Tecnologia de Saneamento Ambiental. Relatório Anual de
736 Qualidade do Ar no Estado de São Paulo 2009, São Paulo, 2010.

737 Chang, J. S., Binkowski, F. S., Seaman, N. L., McHenry, J. N., Samson, P. J.,
738 Stockwell, W. R., Walcek, C. J., Madronich, S., Middleton, P. B., Pleim, J. E.,
739 and Lansford, H. H.: The regional acid deposition model and engineering
740 model, *State-of-Science/Technology, Report 4, National Acid Precipitation*
741 *Assessment Program, Washington, DC, 1989.*

742 Draxler, R. R. and Hess, G. D.: An overview of the HYSPLIT 4 modelling system of
743 trajectories, dispersion, and deposition, *Aust. Meteor. Mag.*, 47, 295-308, 1998.

744 Emmons, L. K., Walters, S., Hess, P. G., Lamarque, F., Pfister, G. G., Fillmore, D.,
745 Granier, C., Guenther, A., Kinnison, D., Laepple, T., Orlando, J., Tie, X.,
746 Tyndall, G., Wiedinmyer, C., Baughcum, S. L., and Kloster, S.: Description
747 and evaluation of the Model for Ozone and Related chemical Tracers, version
748 4 (MOZART-4), *Geosci. Model Dev.*, 3, 43-67, 2010.

749 Ginoux, P., Chin, M., Tegen, I., Prospero, J. M., Holben, B., Dubovik, O., and Lin,
750 S.-J.: Sources and distributions of dust aerosols simulated with the GOCART
751 model, *Journal of Geophysical Research*, 106, 20,255-20,273, 2001.

752 Gong, S. L.: A parameterization of sea-salt aerosol source function for sub- and
753 super-micron particles, *Global Biogeochemical Cycles*, 17, 1097,
754 doi:10.1029/2003GB002079, 2003.

755 Gorin, C. A., Collett, J. L. Jr., and Herckes, P.: Wood smoke contribution to winter
756 aerosol in Fresno, CA, *J. Air & Waste Manag. Assoc.*, 56(11), 1584-1590,
757 2006.

758 GrEC-Grupo de Estudos Climáticos. Relatório climatológico mensal, previsão climática
759 para o Brasil: Set-Out-Nov/2012, Sao Paulo, 2012a. Available at:
760 www.grec.iag.usp.br/link_grec_old/relatorios_climatologicos/2012/agosto/.

761 GrEC-Grupo de Estudos Climáticos. Relatório climatológico mensal, monitoramento
762 climático para o Brasil: Set/2012, Sao Paulo, 2012b. Available at:
763 www.grec.iag.usp.br/link_grec_old/relatorios_climatologicos/2012/setembro/.

764 Grell, G. A., Peckham, S. E., Schmitz, R., McKeen, S. A., Wilczak, J., and Eder, B.:
765 Fully coupled “online” chemistry within the WRF model, *Atmos. Environ.*, 39,
766 6957-6975, 2005.

767 Guenther, A. B., Zimmerman, P. R., Harley, P. C., Monson, R. K., and Fall, R.:
768 Isoprene and monoterpene emission rate variability: model evaluations and
769 sensitivity analyses, *Journal of Geophysical Research*, 98D, 12609-12617,
770 1993.

771 Guenther, A., Zimmerman, P., and Wildermuth, M.: Natural volatile organic
772 compound emission rate estimates for US woodland landscapes, *Atmos.*
773 *Environ.*, 28, 1197-1210, 1994.

774 Fast, J. D., Gustafson, W. I., Easter, R. C., Zaveri, R. A., Barnard, J. C., Chapman,
775 E. G., Grell, G. A., and Peckham, S. E.: Evolution of ozone, particulates, and
776 aerosol direct radiative forcing in the vicinity of Houston using a fully

777 coupled meteorology-chemistry-aerosol module, *Journal of Geophysical*
778 *Research*, 111, D21305, doi:10.1029/2005JD006721, 2006.

779 Forkel, R., Werhahn, J., Hansen, A. B., McKeen, S., Peckham, S., Grell, G., and
780 Suppan, P.: Effect of aerosol-radiation feedback on regional air quality - A
781 case study with WRF/Chem, *Atmospheric Environment*, 53, 202-211, 2012.

782 Heal, M. R., Kumar, P., and Harrison, R. M.: Particles, air quality, policy and health,
783 *Chem. Soc. Rev.*, 41, 6606-6630, 2012.

784 Jenkin, M. E. and Clemitshaw, K. C.: Ozone and other secondary photochemical
785 pollutants: chemical processes governing their formation in the planetary
786 boundary layer, *Atmos. Environ.*, 34, 2499-2527, 2000.

787 Kroll, J. H. and Seinfeld, J. H.: Chemistry of secondary organic aerosol: Formation and
788 evolution of low-volatility organics in the atmosphere, *Atmos. Environ.*, 42,
789 3593-3624, 2008.

790 Kulmala, M., Laaksonen, A., and Pirjola, L.: Parameterization for sulphuric
791 acid/water nucleation rates, *Journal of Geophysical Research*, 103,
792 8301-8307, 1998.

793 Kumar, P., Morawska, L., Birmili, W., Paasonen, P., Hu, M., Kulmala, M., Harrison,
794 R.M., Norford, L., and Britter, R.: Ultrafine particles in cities, *Environment*
795 *International*, 66, 1-10, 2014.

796 Kumar, P., Robins, A., Vardoulakis, S., and Britter, R.: A review of the characteristics
797 of nanoparticles in the urban atmosphere and the prospects for developing
798 regulatory control, *Atmos. Environ.*, 44, 5035-5052, 2010.

799 Kumar, P., Ketzel, M., Vardoulakis, S., Pirjola, L., Britter, R.: Dynamics and dispersion
800 modelling of nanoparticles from road traffic in the urban atmospheric
801 environment - a review, *J. Aerosol Sci.*, 42, 580-603, 2011.

802 Li, G., Bei, N., Tie, X., and Molina, L. T.: Aerosol effects on the photochemistry in
803 Mexico City during MCMA-2006/MILAGRO campaign, *Atmos. Chem. Phys.*,
804 11, 5169-5182, 2011a.

805 Li, G., Zavala, M., Lei, W., Tsimpidi, A. P., Karydis, V. A., Pandis, S. N., Canagaratna,
806 M. R., and Molina, L. T.: Simulations of organic aerosol concentrations in
807 Mexico City using the WRF-Chem model during the
808 MCMA-2006/MILAGRO campaign, *Atmos. Chem. Phys.*, 11, 3789-3809,
809 2011b.

810 Li, G., Zhang, R., and Fan, J.: Impacts of black carbon aerosol on photolysis and
811 ozone, *Journal of Geophysical Research*, 110, D23206,
812 doi:10.1029/2005JD005898, 2005.

813 Marple, V. A., Rubow, K. L., Ananth, G. P., and Fissan, H. J.: Micro-Orifice Uniform
814 Deposit Impactor, *Journal of Aerosol Science*, 17, 489-494, 1986.

815 Martins, L. D., Vasconcellos, P. C., Carvalho, L. F., Andrade, M. F.: Estimated impact of
816 biogenic hydrocarbon emissions on photochemical oxidant formation in Sao Paulo
817 during two periods of the winters of 1999-2000, *Revista Brasileira de Meteorologia*, 21,
818 190-200, 2006.

819 McMurry, P., Shepherd, M., and Vickery, J.: *Particulate Matter Science for Policy*
820 *Makers: A NARSTO Assessment*, Cambridge University Press, Cambridge,
821 England, 2004.

822 Middleton, P., Stockwell, W. R., and Carter, W. P. L.: Aggregation and analysis of
823 volatile organic compound emissions for regional modelling, *Atmos.*
824 *Environ.*, 24A, 1107-1133, 1990.

825 Miranda, R. M. and Andrade, M. F.: Physicochemical characteristics of atmospheric
826 aerosols during winter in the Sao Paulo Metropolitan Area in Brazil, *Atmos.*
827 *Environ.*, 39, 6188-6193, 2005.

828 Monahan, E. C., Spiel, D. E., Davidson, K. L.: A model of marine aerosol generation
829 via whitecaps and wave disruption. In: Monahan, E. C., MacNiocaill, G. D.
830 (Eds.), *Oceanic Whitecaps*. Reidel Publishing Company, Norwell, Mass,
831 167-174, 1986.

832 Muñoz, A. G., López, P., Velásquez, R., Monterrey, L., León, G., Ruiz, F., Recalde,
833 C., Cadena, J., Mejía, R., Paredes, M., Bazo, J., Reyes, C., Carrasco, G.,
834 Castellón, Y., Villarroel, C., Quintana, J., and Urdaneta, A.: An
835 Environmental Watch System for the Andean Countries: El Observatorio
836 Andino, *Bull. Amer. Meteor. Soc.*, 91, 1645-1652, 2010.

837 Muñoz, A. G., Ruiz-Carrascal, D., Ramírez, P., León, G., Quintana, J., Bonilla, A.,
838 Torres, W., Pastén, M., and Sánchez, O.: Risk Management at the Latin
839 American Observatory, in: *Risk Management—Current Issues and Challenges*,
840 InTech Publications, doi:10.5772/50788, 533-556, 2012.

841 Nogueira, T., Dominutti, P. A., De Carvalho, L. R. F., Fornaro, A., and Andrade, M.
842 F.: Formaldehyde and acetaldehyde measurements in urban atmosphere
843 impacted by the use of ethanol biofuel: Metropolitan Area of Sao Paulo,
844 2012-2013, *Fuel*, 134, 505-513, 2014.

845 Odum, J. R., Hoffmann, T., Bowman, F., Collins, D., Flagan, R. C., and Seinfeld, J.
846 H.: Gas/particle partitioning and secondary organic aerosol yields,
847 *Environmental Science Technology*, 30, 2580-2585, 1996.

848 Pankow, J. F.: An absorption model of the gas aerosol partitioning involved in the
849 formation of secondary organic aerosol, *Atmos. Environ.*, 28, 185-188, 1994a.

850 Pankow, J. F.: An absorption model of the gas aerosol partitioning involved in the
851 formation of secondary organic aerosol, *Atmos. Environ.*, 28, 189-93, 1994b.

852 Pérez-Martínez, P. J., Andrade, M. F., and Miranda, R. M.: Traffic-related air quality
853 trends in Sao Paulo, Brazil, *J. Geophys. Res. Atmos.*, 120, 6290-6304,
854 doi:10.1002/2014JD022812, 2015.

855 Pérez-Martínez, P. J., Miranda, R. M., Nogueira, T., Guardani, M. L., Fornaro, A.,
856 Ynoue, R., and Andrade, M. F.: Emission factors of air pollutants from
857 vehicles measured inside road tunnels in Sao Paulo: case study comparison,
858 *Int. J. Environ. Sci. Technol.*, 11, 2155-2168, 2014.

859 Real, E. and Sartelet, K.: Modelling of photolysis rates over Europe: impact on
860 chemical gaseous species and aerosols, *Atmos. Chem. Phys.*, 11, 1711-1727,
861 2011.

862 Salvo, A. and Geiger, F. M.: Reduction in local ozone levels in urban Sao Paulo due to a
863 shift from ethanol to gasoline use, *Nature Geoscience*, 7, 450-458,
864 doi:10.1038/ngeo2144, 2014.

865 Saxena, P., Hudischewskyj, A. B., Seigneur, C., and Seinfeld, J. H.: A comparative
866 study of equilibrium approaches to the chemical characterization of
867 secondary aerosols, *Atmos. Environ.*, 20, 1471-1483, 1986.

868 Schell, B., Ackerman, I. J., Hass, H., Binkowski, F. S., and Ebel, A.: Modelling the
869 formation of secondary organic aerosol within a comprehensive air quality
870 model system, *Journal of Geophysical Research*, 106, 28275-28293, 2001.

871 Seinfeld, J. H. and Pandis, S. N.: *Atmospheric Chemistry and Physics: from air*
872 *pollution to climate change*, Second Edition, Jhon Wiley, New Jersey,
873 2006.

874 Shrivastava, M., Berg, L. K., Fast, J. F., Easter, R. C., Laskin, A., Chapman, E. G.,
875 Gustafson Jr, W. I., Liu, Y., and Berkowitz, C. M.: Modelling aerosols and
876 their interactions with shallow cumuli during the 2007 CHAPS field study,
877 *Journal of Geophysical Research: Atmospheres*, 118, 1343-1360, 2013.

878 Taylor, K. E.: Summarizing multiple aspects of model performance in a single diagram,
879 *Journal of Geophysical Research*, 106(D7), 7183-7192,
880 doi:10.1029/2000JD900719, 2001.

881 Tuccella, P., Curci, G., Visconti, G., Bessagnet, B., Menut, L., and Park, R. J.:
882 Modelling of gas and aerosol with WRF-Chem over Europe: Evaluation and
883 sensitivity study, *Journal of Geophysical Research*, 117, D03303,
884 doi:10.1029/2011JD016302, 2012.

885 Vasconcellos, P. C., Souza, D. Z., Sanchez-Ccoyllo, O. R., Bustillos, J. O. V., Lee,
886 H., Santos, F. C., Nascimento, K. H., Araujo, M. P., Saarnio, K., Teinila, K.,
887 and Hillamo, R.: Determination of anthropogenic and biogenic
888 compounds on atmospheric aerosol collected in urban, biomass burning
889 and forest areas in Sao Paulo, Brazil, *Science of the Total Environment*, 408,
890 5836-5844, 2010.

891 Vieira-Filho, M. S., Pedrotti, J. J., and Fornaro, A.: Contribution of long and mid-range
892 transport on the sodium and potassium concentrations in rainwater samples, Sao
893 Paulo megacity, Brazil, *Atmos. Environ.*, 79, 299-307, 2013.

894 Wedding, J. B., Weigand, M., John, W., and Wall, S.: Sampling effectiveness of the inlet
895 to the dichotomous sampler, *Environ. Sci. Technol.*, 14(11), 1367-1370, 1980.

896 Ynoue, R. Y. and Andrade, M. F.: Size-resolved mass balance of aerosol particles over
897 the Sao Paulo Metropolitan Area of Brazil, *Aerosol Science and Technology*, 1,
898 52-62, 2004.

899 Table 1. Description of aerosol sampling campaigns performed at IAG-USP.

Parameter	Sampling frequency	Period of sampling	Sampling device
Aerosol mass size distribution	24 hours	July-September	MOUDI impactor
PM _{2.5} and PM ₁₀ concentration	12 hours	July-September	Dichotomous sampler
OC and EC concentration	12 hours	August-September	Sunset OC-EC analyser

900

901

902 Table 2. Description of measurement sites.

Site	Initials	Latitude	Longitude	Classification	Measured species
Nossa S. do Santana	NSO	-23.4796	-46.6916	Urban	PM ₁₀ , O ₃
Parque D. Mooca	PDP	-23.5448	-46.6276	Urban	PM ₁₀ , O ₃
Cerqueira IAG-USP	MOO	-23.5497	-46.5984	Urban	PM ₁₀ , O ₃
	CCE	-23.5531	-46.6723	Urban	PM ₁₀
	IAG-USP	-23.5590	-46.7330	Suburban	PM ₁₀ , PM _{2.5} , OC, EC, aerosol mass size distrib. ^a
IPEN-USP	IPEN-USP	-23.5662	-46.7374	Suburban	PM _{2.5} , O ₃ , NO _x , CO
Ibirapuera	IBI	-23.5914	-46.6602	Suburban	PM ₁₀ , O ₃ , NO _x , CO
Congonhas	CON	-23.6159	-46.6630	Urban	PM ₁₀ , PM _{2.5}
AF-IAG	AF-IAG	-23.6500	-46.6167	Suburban	T, RH, WS, WD ^b
Santo	SAM	-23.6545	-46.7095	Urban	PM ₁₀
Interlagos	INT	-23.6805	-46.6750	Urban	PM ₁₀ , O ₃ , T, RH, WS, WD

903 ^aincludes SO₄²⁻, NO₃⁻, NH₄⁺, Na⁺, Cl⁻ and PM₁₀.

904 ^bT, RH, WS, and WD denote temperature, relative humidity, wind speed and wind
 905 direction, respectively.

906

907 Table 3. Selected WRF-Chem configuration options.

Atmospheric Process	WRF-Chem option
Longwave radiation	RRTM
Shortwave radiation	Goddard
Surface layer	Monin-Obukhov
Land surface	Noah
Boundary layer	YSU
Cumulus clouds ^a	Grell 3D
Cloud microphysics	Lin
Gas-phase chemistry	RADM2
Aerosol chemistry	MADE/SORGAM
Photolysis	Fast-J

908 ^aOuter domains only

909

910 Table 4. Description of WRF-Chem simulations.

Label	Description
Case_0 (Baseline simulation)	Emission of gases Emission of aerosols Aerosol-radiation feedback turned on
Case_1	Emission of gases No emission of aerosols Aerosol-radiation feedback turned on
Case_2	Emission of gases Emission of aerosols Aerosol-radiation feedback turned off

911

912

913 Table 5. Performance statistics for WRF-Chem predictions at all sites^a

Index	PM _{2.5}	PM ₁₀	O ₃	NO _x	CO	T	RH	WS	WD
MB	-8.84	-14.10	-0.85	-8.75	-0.27	0.65	-5.74	0.54	31.12
MFB (%)	-47.62	-38.19	22.63	12.68	-32.53	1.94	-7.95	41.21	31.66
MFE (%)	47.90	39.90	72.85	82.82	80.93	14.16	23.84	71.12	54.40
RMSE _{UB}	6.83	10.59	27.45	30.35	0.57	3.21	20.06	1.08	79.38
R	0.73	0.72	0.63	0.42	0.54	0.71	0.62	0.41	0.43

914 ^aValues are averaged from all the individual indexes found at the measurement sites.

915 Individual indexes are calculated from both hourly observed and predicted values.

916 Figure 1. Downtown area of the 3 km modelling domain (d03) showing the locations of
917 measurement sites and WRF topography in the vicinity of the SPMA. Red dots
918 represent sites with information on O₃ and PM. Yellow dots represent only
919 sites with information on PM. Blue dot represents the location of the IAG-USP's
920 climatological station.

921 Figure 2. Emission rates for Aromatic VOCs at 19 UTC in the 3 km modelling
922 domain.

923 Figure 3. Hourly accumulated precipitation and relative humidity observed at the
924 IAG-USP's climatological station during the study period.

925 Figure 4. HYSPLIT three-day backward trajectories and locations of fires in Sao Paulo
926 State and part of central-west region of Brazil. Pink markers represent the
927 observed fire locations during the study period considering different satellite
928 products (GOES, AQUA, TERRA, NOAA). The backward trajectories starting
929 at IAG-USP were calculated for the days 9 and 31 August and 5 September 2012
930 at three different altitudes: 500 m (red lines), 1000 m (blue lines), and 2000 m
931 (green lines).

932 Figure 5. Daily (top), diurnal (bottom), and nocturnal (middle) mean concentrations for
933 EC, OC, PM₁₀, PM_{2.5-10}, PM_{2.5} (left panels), and Na, Fe₂SO₃, SiO₂, K₂O, and S
934 (right panels). The PM_{2.5-10} aerosol variable is defined as particulate matter with
935 aerodynamic diameter between 2.5 and 10 μm. The grey line indicates the WHO
936 air quality standard for PM_{2.5} (25 μg m⁻³).

937 Figure 6. The predicted average of wind vectors at 10 m and temperature at 2 m from
938 the baseline simulation (Case_0) for the whole study period in the 3 km
939 modelling domain. Blue dots represent the locations of the measurement sites,

940 whereas cyan numbers represent the observed average temperature in those
941 sites: 17.7 °C in AF-IAG and 17.8 °C in INT.

942 Figure 7. The observed and predicted daily variations of PM_{2.5} concentrations at three
943 sites in SPMA for the 3 km modelling domain.

944 Figure 8. The observed and predicted daily variations of PM₁₀ concentrations at ten sites
945 in SPMA for the 3 km modelling domain.

946 Figure 9. The observed and predicted hourly variations of O₃ concentrations at six sites
947 in SPMA for the 3 km modelling domain.

948 Figure 10. Taylor diagram (Taylor, 2001) showing the individual correlation
949 coefficients, mean biases, and normalized standard deviations for the PM₁₀, PM_{2.5}, OC
950 and EC concentrations.

951 Figure 11. The predicted average surface distribution of PM_{2.5} concentrations for the
952 whole study period in the 3 km modelling domain. Red dots represent the
953 locations of the measurement sites with information on PM_{2.5}, whereas cyan
954 numbers represent the observed average PM_{2.5} concentration in those sites: 23.4
955 µg m⁻³ in IPEN-USP, 21.3 µg m⁻³ in IAG-USP, and 22.2 µg m⁻³ in CON.

956 Figure 12. The predicted average surface distribution of PM₁₀ concentrations for the
957 whole study period in the 3 km modelling domain. Red dots represent the
958 locations of the measurement sites with information on PM₁₀, whereas cyan
959 numbers represent the observed average PM₁₀ concentration in those sites: 49.5
960 µg m⁻³ in IAG-USP and 38.7 µg m⁻³ in CON.

961 Figure 13. The predicted average surface distribution of the PM_{2.5}:PM₁₀ ratio for the
962 whole study period in the 3 km modelling domain. Red dots represent the
963 locations of the measurement sites with information on both PM_{2.5} and PM₁₀,

964 whereas cyan numbers represent the observed average $PM_{2.5}:PM_{10}$ ratio in those
965 sites: 0.43 in IAG-USP and 0.57 in CON.

966 Figure 14. The observed and predicted daily variations of OC and EC concentrations
967 at IAG-USP.

968 Figure 15. The observed and predicted average aerosol mass size distribution for SO_4 ,
969 NO_3 , NH_4 , Na, Cl, and other PM_{10} constituents at IAG-USP. The observed
970 aerosol distributions were collected in ten size classes using a rotated impactor
971 (MOUDI) and joined adequately according to the three modes used by the
972 MADE aerosol scheme: Aitken ($<0.1 \mu m$), accumulation ($0.1-1 \mu m$) and coarse
973 ($>1 \mu m$). The five inorganic ions carried in MADE are only calculated for the
974 Aitken and accumulation modes. The WRF's PM_{10} aerosol variable does not
975 include neither OC nor EC for this comparison.

976 Figure 16. The observed and predicted average contributions for the main identified
977 constituents of $PM_{2.5}$ at IAG-USP.

978 Figure 17. The impact of (a) emissions of primary gases on the fine particles formation,
979 (b) emissions of dust-sea salt aerosols on the PM_{10} concentration, and (c) aerosol
980 direct effect on the ground level O_3 concentrations at 16:00 h (local time).